a Ph.D. degree in physics from the University of Denver, CO, in 1971.

He was a Research Associate and a Physics Instructor at the University of Denver from 1971 until March 1973, when he joined the University of Brussels and the International (Solvay) Institute of Physics and Chemistry, Brussels, Belgium, where he was engaged in the basic research in irreversible thermodynamics and nonequilibrium statistical mechanics. He returned to the United States at the end of 1976 to join Tracor, Inc., as a Senior Scientist in its Rockville Laboratory, MD, and directed the Research and Development in quantum optics and fiber optics. From 1978 to 1983, he was with IIT Research Institute, Annapolis, MD, where he was engaged in basic and applied research of quantum electronics, nonsteady state physics and irreversible thermodynamics, transient dielectric interactions, and microwave medical physics. Since February 1983, he has been with the Johns Hopkins University Applied Physics Laboratory Laurel, MD, and has continued the research in these subjects.

✤

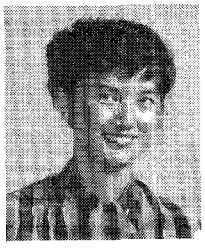

Wendy W. Guo (SM'79) graduated from Chung-Yuan College of Sciences and Engineering, Taiwan, in 1968 with a B.S. degree in chemistry, and received the M.S. and Ph.D. degrees in physics from the University of Denver, CO, in 1970 and 1973, respectively.

Between 1973 and 1976, she was a Research Physicist in the University of Brussels and International (Solvay) Institute of Physics and Chemistry, Brussels, Belgium, where she was involved in the basic research of irreversible thermodynamics and nonequilibrium statistical physics. From 1976 to 1978, she was a Senior Scientist in Tracor, Inc., Rochville, MD. From 1978 to 1983, she was a Senior Research Engineer in IIT Research Institute, Annapolis, MD, where she was engaged in a number of projects concerning basic and applied research of transient dielectric interactions in condensed matters and nonsteady-state physics, microwave interaction in biological systems, electromagnetic theory, and adaptive array and radar analysis. Since February 1983, she has been with the Applied Physics Laboratory, Johns Hopkins University, Laurel, MD, where she has beeen performing research in thermodynamics and statistical physics with respect to the transient state interaction of radiation and matter, thermal properties of microwave interaction with biological materials, and application of microwave physics in medicine.

✤

Lawrence Edwin Larsen (M'81–SM'82) attended and received the M.D. degree magna cum laude from the University of Colorado, Fort Collins, in 1968. He was awarded an NIH postdoctoral fellowship in biophysics at UCLA for the period 1968–1970.

He then served in the United States Army as a Research Physiologist in the Department of Microwave Research at the Walter Reed Army Institute of Research during 1970–1973. From 1973 to 1975, he accepted a faculty appointment in the Radiology Department at the Baylor College of Medicine in Houston, TX, where he taught physiology and computer sciences. In 1975, he returned to the Walter Reed Army Institute of Research as the Associate Chief of Microwave Research. He was appointed the Department Chief in 1977 and presently serves in that role with the rank of Colonel, Medical Corps. He holds several patents.

Microwave Thermoelastic Tissue Imaging—System Design

JAMES C. LIN, SENIOR MEMBER, IEEE, AND KAREN H. CHAN

Abstract—**A microwave-induced thermoelastic tissue imaging system is proposed as a new and promising imaging modality. It possesses unique features that permit noninvasive imaging of tissue characteristics which are not identifiable by other techniques. It uses nonionizing radiation and relies on a beam of impinging microwave energy to launch an acoustic wavefront into tissue. This thermoelastic wave of pressure propagates through the tissue and is detected by a two-dimensional array of piezoelectric transducers positioned on the body surface to give an image of the intervening tissue structure. Signals from the output of this transducer array are amplified and band-limited. A computer-controlled data acquisition system samples and converts them to digital form for further processing. A hybrid parallel/serial design for dividing the array into segments and collecting data from each segment sequentially is used. The area image sensor offers inherent geometric stability essential for reliable measurement. Error in scan position is not a concern, since mechanical scanning is not involved. The gray level resolution is 256 after digitization, and the spatial resolution is 5×5 mm. These resolutions, along with a calculated signal-to-noise ratio greater than 2500, are sufficient to provide structural information needed to render microwave-induced thermoelastic imaging a useful, noninvasive method for imaging biological tissues.**

Manuscript received October 12, 1983; revised March 11, 1984. This work was supported in part by the National Science Foundation and the Office of Naval Research.

The authors are with the Department of Bioengineering, University of Illinois at Chicago, P.O. Box 4348, Chicago, IL 60680.

I. Introduction

THE LAST DECADE has witnessed tremendous advances in the field of biomedical imaging. Imaging modalities and protocols which only a short time ago were in the experimental stage have, during the last decade, become routine clinical procedures. In hematology, for example, automated instruments process blood slides on a daily basis in the clinical laboratory. In nuclear medicine, nuclear image processors are used in perform over 7 million scintigraphic studies yearly in the U.S. In cardiology, real-time ultrasonic systems are used routinely to image

0018-9480/84/0800-0854$01.00 ©1984 IEEE

moving organs and represent a steadily growing field in diagnostic radiology. Finally, the development of X-ray and nuclear magnetic resonance computed tomography is unquestionably the most significant advancement in the diagnostic imaging field since the discovery of X-ray [1], [2].

These noninvasive techniques measure different biophysical parameters of the body with differing sensitivity for pathophysiological processes. Each technique has its own potentials and limitations. Nevertheless, the success of these techniques has prompted a number of researchers to explore other physical and chemical properties of biological materials for noninvasive tissue characterization. Microwave-induced thermoelastic waves appear to possess some unique features that may allow them to become as useful as these other methods and to permit noninvasive imaging of tissue characteristics which are not identifiable by other techniques. Specifically, there is a direct relation between the pattern of absorbed microwave pulses and the induced thermoelastic pressure waves in biological tissues [3]. Moreover, regions of differing permittivity would exhibit differential absorption. Thus, a brief burst of microwave pulses could provide either deep, surface, or wide-area acoustic illumination, according to a selected microwave absorption pattern. The microwave-induced thermoelastic pressure wave could then be received by a two-dimensional array of acoustic transducers and digitally processed to generate thermoelastic images of the irradiated region. This unique feature may become a valuable adjunct to density and acoustic impedance characteristics of X-ray and ultrasonic imaging in identifying pathophysiologic states [4], [5].

In this paper, a design for a microwave-induced thermoelastic tissue imaging system, along with an example which demonstrates one possible application of the design, is presented.

II. Thermoelastic Signal Propagation

When a beam of microwave energy impinges normally on the boundary of a semi-infinite region of homogeneous tissue material, a portion of the incident radiation is absorbed by the tissue and converted into heat which generates a temperature gradient normal to the surface. As a result of thermal expansion occurring within a few microseconds (duration of a short pulse), this temperature produces strains in the tissue material and leads to generation of stress waves which propagate away from the surface. Fig. 1 shows a typical bell-shaped microwave-induced displacement curve. A complete analysis of the displacement and pressure generated by microwave-induced thermoelastic expansion in semi-infinite medium is given in [7], [8]. The elastic wave energy produced is characterized by the following equation:

$$E_a = \frac{A_a C \beta^2 I_0^2}{2\pi J^2 S^2} \frac{\left(1 - e^{-\alpha_t C T_0} - \alpha_t C T_0 e^{-\alpha_t C T_0}\right)}{\alpha_t C} \qquad (1)$$

where the parameters are explained in Table I.

As this acoustic wave propagates inside the tissue, attenuation occurs which is assumed to be exponential.

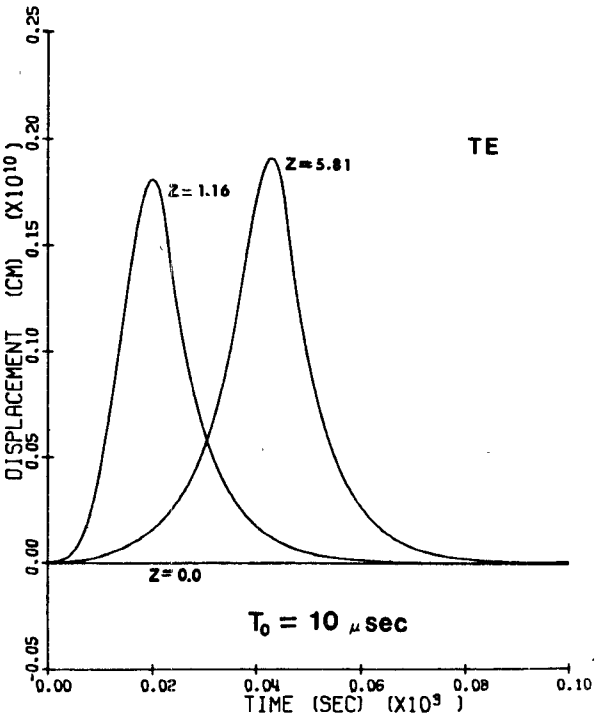

Fig. 1. A typical bell-shaped microwave-induced displacement curve.

TABLE I
Parameters for S/N Calculation

Symbol	Explanation & Source of Reference	Data Used for Calculation
A_a	Area through which the elastic wave is propagated	10 cm x 10 cm = 0.01 m^2
$I_o^2 A_a$	maximum power output from a microwave pulse generator (EPSCO pH 40K)	10 KW
C	velocity of elastic wave propagation for muscle at 37 C (1, p. 108)	1575-1585 m/s (use: 1580 m/s)
β	coefficient of thermal expansion ($°C^{-1}$) (1, p. 111)	4.14 x 10(-5)/°C
ρ	density of muscle at 37 C (1, p. 108)	1070 Kg/m^3
J	mechanical equivalent of heat	4.186 J/cal
S	specific heat of muscle (1, p. 111)	750 cal/Kg C
α_t	attenuation coefficient of microwave in muscle at 2450 MHz (1, p. 109)	0.6 x 2/cm = 120/m
T_0	pulse width	25μs
α_a	attenuation coefficient of thermal elastic wave at 1 MHz (1)	13-25/m x 2 (use: 26/m)

Therefore, the energy received at the piezoelectric transducer is $E_a' = E_a e^{-\alpha_a x}$, where α_a is the attenuation coefficient of the propagating acoustic wave and x is the distance travelled.

With the parameters from Table I, we obtain

$$E_a = 6.43 \times 10^{-12} \text{ J}$$

and

$$E_a' = 4.78 \times 10^{-13} \text{ J}$$

for the elastic wave energy at $x = 0$ and 10 cm, respectively.

III. System Design

A block diagram of the thermoelastic imaging system is shown in Fig. 2. Major components of the system include a microwave pulse generator, a piezoelectric receiving transducer array, a signal conditioning and data conversion interface, and a processing and control computer with graphic display capability. The transducers detect the intensity of the thermoelastic wave. The signal conditioning and data conversion system conditions and translates the signals into a set of numerically coded values in a format acceptable to the computer.

Current signals received from the transducer array are first amplified and converted to voltages of useful level (full-scale range of an A/D converter is normally -10 to 10V). The signals then pass through a filtering section to band-limit the frequency components to avoid aliasing and to reduce high-frequency noise. The processed analog signals pass to sample-hold circuits, which acquire the signal voltages and hold their values, while an analog-to-digital converter converts these values into digital form. The resultant digital words are transmitted to a computer data base for storage and further processing.

The system is designed with the capability of imaging heart motion. According to the well-known Nyquist criterion of the sampling theorem, the signal must be sampled at least twice as fast as its highest frequency component in order to recover this band-limited signal without distortion. The minimum sampling time is thus set to 2.5 ms. Different design approaches for data acquisition will be discussed. A parallel design is the most efficient, but it is also the most expensive. A serial design is limited by present technology. A hybrid parallel/serial design of dividing the 20×20 array into segments and collecting data from the segments is suggested.

In the following section, specific design details on the data acquisition system are provided.

IV. Data Acquisition System

The main functions of the data acquisition system consist of signal detection, amplification, filtering, digital conversion and transmitting the digital data to the computer for further data manipulation.

A. Signal Detection

The acoustic signal is received by a 20×20 piezoelectric transducer array. The transducer array consists of lead zirconate titanate and has a free-field voltage sensitivity of -220 db at 70 KHz. The array is sealed within a square metal frame that measures 21 cm on a side. The area image sensors offer inherent geometric stability essential for reliable measurement. Scan position error is minimal since it does not involve scanning.

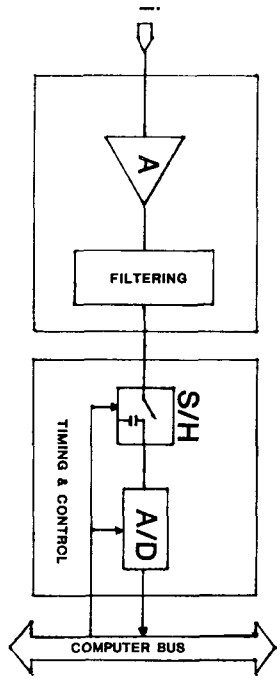

Fig. 2. A block diagram of the thermoelastic tissue imaging system.

B. Signal Amplification

Piezoelectric materials have high but finite resistance. As a result, the charge generated by an applied force leaks through the leakage resistor, causing the potential difference eventually to reduce to zero. The attachment of a voltage amplifier to the output of the transducer will degrade the transducer characteristics if the input impedance of the voltage amplifier is not at least an order of magnitude higher than that of the piezoelectric transducer. The resistance of a piezoelectric transducer is typically on the order of 100 GΩ. The usual input resistance becomes important, causing charge to be lost and thereby decreasing the output voltage.

In order to improve the dynamic response of the transducer at low and medium frequencies, the output of the piezoelectric transducer is fed directly into the negative input of a charge amplifier (Fig. 3) [7]. There is a virtual ground at the negative input to the amplifier. Theoretically, current generated by the transducer all flows into the feedback capacitor and no current goes through the input resistor or the input capacitor. However, the op-amp bias current causes the charge amplifier to drift slowly with time. Therefore, the large feedback resistor R_f is added to the system to avoid saturation problems.

C. Signal Filtering

The equivalent circuit for a piezoelectric transducer at high frequency is more complex due to its mechanical resonance. The dynamic response of the transducer at high frequencies is not a simple linear function. In order to avoid aliasing and high-frequency noise, a filtering section is introduced to band-limit the signal. Previous experiments have shown that the frequency range of the transducer is linear—approximately between 25 to 250 KHz [5].

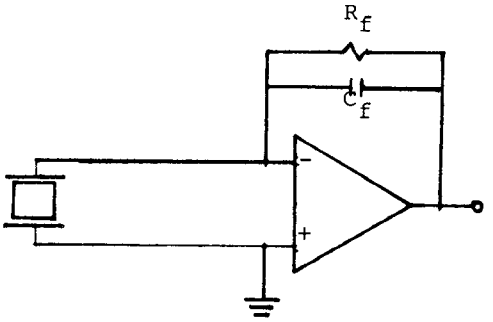

Fig. 3. A charge amplifier.

A band-pass filter with cutoff frequencies of 25 and 250 KHz is selected. The overall bandwidth of the filter is 225 KHz, while the percentage bandwidth is 285 percent. Since the percentage bandwidth is more than 80 to 100 percent, an overlapping high-pass and low-pass cascaded filter is desirable. Active filters have many advantages over the traditional passive filters. However, the frequency response attainable within present technology is limited to about 50 KHz. For this application, passive filters were chosen (Fig. 4).

D. Data Conversion

The need for acquiring images of good resolution, low noise, and minimal motion artifact imposes requirements on the electronic circuitry of the data conversion devices, including sample-holds (S/H), analog-to-digital converters (ADC), etc. The maximum value of input signal frequency that can be acquired and digitized using a serial combination of S/H and ADC is not only influenced by the bandwidth of the S/H, but is also dictated by the aperture uncertainty of the S/H, plus the desired accuracy and corresponding resolution of the converter. The images are digitized into 256 gray levels, which correspond to 8 bits resolution of the ADC. Sample-holds with aperture uncertainty t_u of 5 ns and ADC of 8 bits resolution have a maximum input signal acquisition frequency of 250 KHz (Analog Device, [8, pp. 14–20]). A number of design approaches are available to take advantage of this signal acquisition rate.

1) Parallel Design: A complete parallel design for the microwave thermoelastic tissue imaging system simply means 400 signal transducer systems, or 400 S/H's and 400 ADC's. Fig. 5 shows a block diagram of this design. The sampling time t_s is equal to the sum of the acquisition time of the sample-holds $t_{S/H}$ and the conversion time t_{con} or

$$t_s = t_{con} + t_{S/H} \leqslant 2.5 \text{ ms}. \tag{2}$$

Sample-holds and analog-to-digital converters that satisfy this requirement are commercially available. However, the cost of the design is extremely large because it includes 400 sample-holds and 400 analog-to-digital converters. In fact, 400 ADC's are redundant. They can be replaced by 25–16 $\times 1$ analog multiplexers and one fast analog-to-digital converter. A block diagram of this modified design is shown in

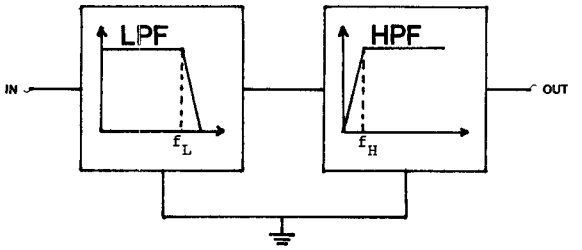

Fig. 4. A cascaded low-pass, high-pass passive filter.

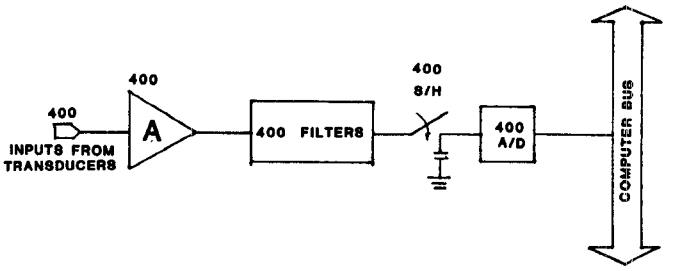

Fig. 5. A block diagram of a parallel system.

Fig. 6. The sampling time equation and the cost are changed accordingly. Equation (2) will become

$$t_s = t_{S/H} + 400t_{con} \leqslant 2.5 \text{ ms}. \tag{3}$$

Again, timing is not a problem for a modified parallel design. The cost goes down slightly, but it remains a costly system.

2) Serial Design: At another extreme, 25–16$\times$1 analog multiplexers are used to present the transducer outputs serially to the sample-holds and analog-to-digital circuit. Fig. 7 is a block diagram illustrating this design. The cost of the system is reduced tremendously. However, the time available for the acoustic signals to be collected by the transducers is very short (approximately 20 μs). In order to detect a pulse at the 400th transducer before it passes away, the sampling time from the first transducer to the 400th transducer t_{400} must be less than 20 μs

$$t_{400} = 400xt_{MUX} + 399x(t_{S/H} + t_{ADC}) \tag{4}$$

where t_{MUX} is the delay time of the analog multiplexer from the enable input to the switch "ON" or "OFF" condition. There is no commercially available combination of multiplexers, sample-holds, and analog-to-digital converters which can achieve an acquisition time close to 50 ns. Therefore, even though this design is economical, it is limited by the present technology. Thus, both the parallel and serial designs have their advantages and limitations.

3) Hybrid Parallel/Serial Design: A hybrid parallel/serial design is suggested to include advantages of both previous designs and to avoid their disadvantages and limitations. The array is segmented into different regions, as shown in Fig. 8. Data are collected from each segment sequentially. N is desired to be an integer which can divide 20. Therefore, $N = (1,2,4,5,10,20)$. Fig. 9 is a block diagram of this hybrid design. N^2 channels are selected by the first-level analog multiplexers to present the outputs of the transducers to N^2 sample holds. Only one channel out of

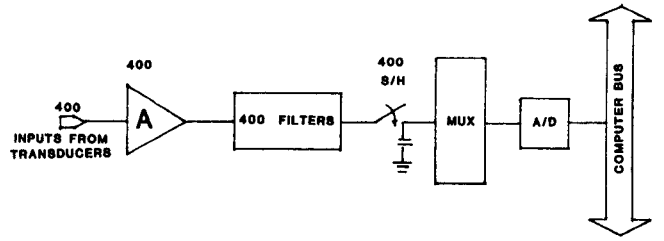

Fig. 6. A block diagram of a modified parallel system.

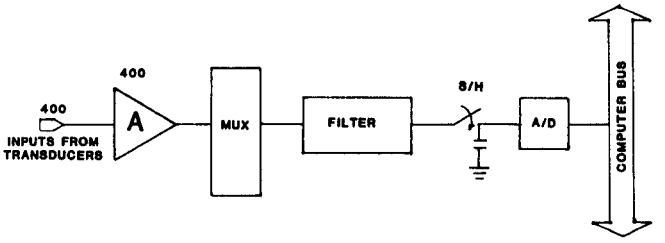

Fig. 7. A block diagram of a serial system.

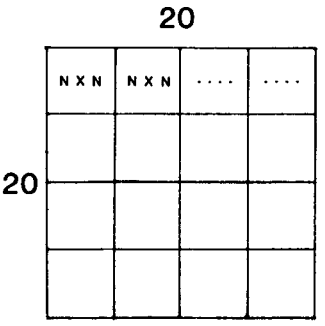

Fig. 8. Picture segmentation.

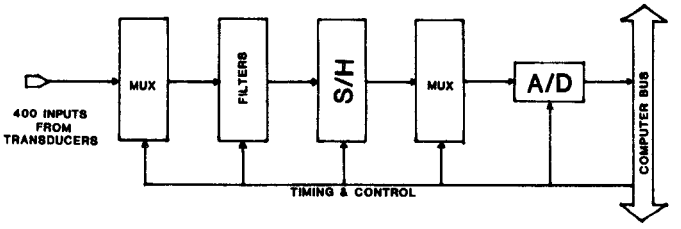

Fig. 9. A block diagram of a hybrid parallel/serial system.

N^2 sampled values is selected by the second-level multiplexing. Table II lists some of the possible numbers of multiplexers for different values of N.

The microwave pulse generator produces M successive microwave pulses which impinge on the phantom. For each pulse, N^2 data are collected by a microcomputer. M is equal to the divident of 400 by N ($M = 400/N$). The sampling time is equal to

$$t_s = t_{\mathrm{MUX}} + t_{\mathrm{S/H}} + (t_{\mathrm{MUX}} + t_{\mathrm{ADC}}) * N^2. \quad (5)$$

All N^2 conversions have to be finished within a pulse period T ($t_s \leqslant 2.5$ ms). The maximum droop error for each sample hold is determined by the maximum "hold" time of the system, which is established by the analog-to-digital conversion rate and the number of data channels. Droop

TABLE II
PARAMETERS FOR HYBRID PARALLEL/SERIAL DESIGN

N	M	Number Of Multiplexers For First Level Multiplexing	Second Level Multiplexing
1	400	25	0
2	100	25	1
4	25	25	1
5	16	25	2
10	4	25	7
20	1	0	25

error is computed as: maximum droop error $= t_{\mathrm{ADC}} * N^2$. The droop rate is defined as the product of this maximum droop error and the sampling time. In order to maintain the gray level resolution desired, this droop rate must be appreciably less than 1/2 the least significant bit (LSB) of an analog-to-digital converter. The cost varies as a function of N. The following example is included to demonstrate one possible application of this design.

4) An Example: When $N = 1$, it is equivalent to sampling 400 points by moving a single transducer and applying a pulse at each sample point. The cost is minimum, but 400 microwave pulses are needed for each picture frame. When $N = 20$, the design is identical to the modified parallel system. Therefore, $N = 5$ is chosen for optimizing the cost and the number of microwave pulses per picture frame. The first-level and second-level multiplexing, using twenty-five and two 16-channel analog multiplexers, respectively, are implemented. Twenty-five samples are held simultaneously by twenty-five sample-holds placed after the first-level multiplexing. A fast analog-to-digital converter converts voltages at the sample-hold outputs into binary coded numbers serially. Sixteen pulses are needed to collect a complete picture frame. If an analog-to-digital converter with 15-μs conversion time is used for 25 samples, a sampling time of 500 μs can be achieved. For sample-holds with a droop rate less than 5 mV/s, the maximum droop error should not exceed 25 μV. The analog voltage corresponding to the LSB of an 8-bit analog-to-digital converter is about 78 mV. The droop error is around 0.03 percent with respect to the analog voltage of the LSB code. It is certainly insignificant.

The control circuit for synchronizing the whole process is the most crucial part of the system design. It is impossible to estimate the exact time for a microwave pulse to travel through the media, generate an acoustic signal, reach the phantom, and finally be detected by the transducers. A transducer by the side, which is least interfered with by the phantom, is chosen to monitor this timing. A signal received by this transducer passes through a circuit (Fig. 10) to generate a digital control signal to sample-holds, and to signify the computer outputting command to the analog-to-digital converter to start conversion. The computer reads

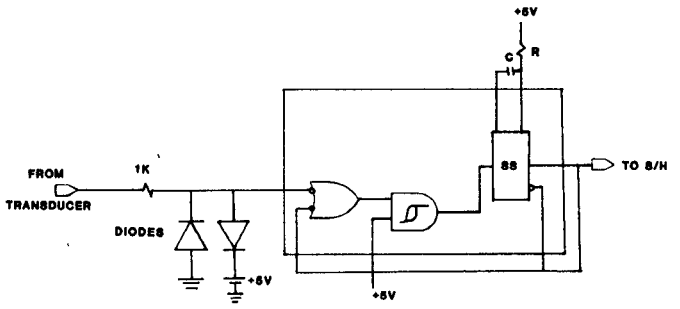

Fig. 10. The control circuit of the data acquisition system.

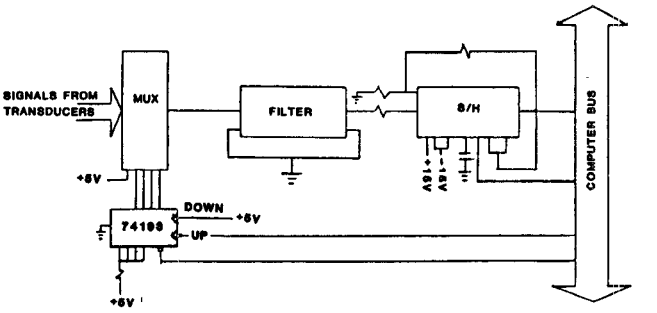

Fig. 11. Schematic diagram for the microwave-induced thermoelastic imaging system.

the data and stores it in memory at the completion of a conversion. The computer then instructs the analog-to-digital converter to start another conversion. At the end of the 25th data reading, the computer outputs a signal to the microwave pulse generator to deliver another pulse to the phantom. The process repeats sixteen times to complete one picture frame. Figs. 11 and 12 show the schematic diagrams for this system design.

V. Signal-to-Noise Calculation

The main source of noise for this detecting system is electronic noise, which includes thermal noise, shot noise, amplifier noise, etc. In the noise power calculation, it is assumed that thermal and amplifier noise are the predominate noise affecting the circuit.

Thermal noise is due to electrons moving randomly about in resistive material due to thermal agitation. It's power varies proportionally to its bandwidth. Equation (6) describes the thermal power spectrum [9]

$$E_n^2 = 4kT\int_B \mathrm{Re}(f)\,df \tag{6}$$

where

k Boltzmann's constant
T absolute temperature in Kelvin,
$\mathrm{Re}(f)$ the real part of the circuit impedance.

The thermal noise for an RC parallel network is equal to

$$E_n^2 = \frac{4kT}{2\pi C}\left(\tan^{-1}\omega_H RC - \tan^{-1}\omega_L RC\right). \tag{7}$$

The total thermal noise at the output of the charge amplifier is

$$E_{\text{thermal}}^2 = \frac{2kT}{\pi C_i}\left(\tan^{-1}\omega_H R_i C_i - \tan^{-1}\omega_L R_i C_i\right)G^2 + \frac{2kT}{\pi C_f}\left(\tan^{-1}\omega_H R_f C_f - \tan^{-1}\omega_L R_f C_f\right) \tag{8}$$

where G = gain of the circuit. The other parameters are explained in Table I.

The amplifier noise is usually specified by the manufacturer as an equivalent voltage or current source at the input of the amplifier.

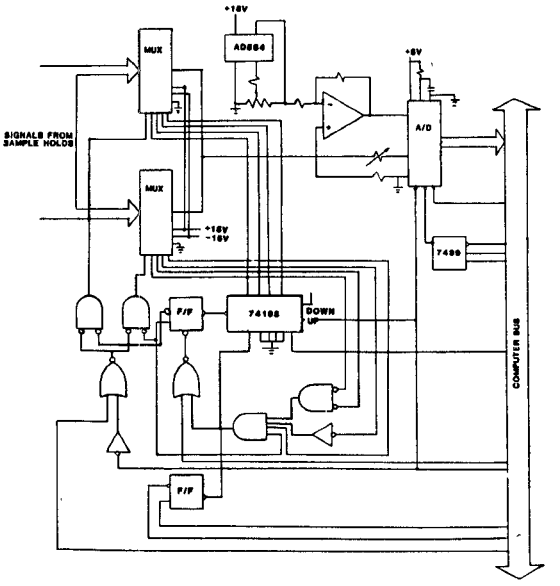

Fig. 12. Schematic diagram for the microwave-induced thermoelastic imaging system.

The total squared noise voltage is given by

$$\bar{E}_{\text{total}}^2 = E_{\text{thermal}}^2 + \bar{V}_n^2 G^2. \tag{9}$$

The noise power per hertz at the end of this stage is

$$\left(\bar{E}_{\text{total}}^2/Z_L\right) = \frac{\bar{E}_{\text{total}}^2 2\pi C_f\left(f_{H_L} - f_{L_L}\right)}{\tan^{-1}\omega_{H_L} R_f C_f - \tan^{-1}\omega_{L_L} R_f C_f}. \tag{10}$$

It is well known from signal detection theory [10] that, in the presence of noise, the output of a matched filter is given by S/N

$$\mathrm{S/N} = \left\{2\int_0 \left(E_a(t)\right)^2 dt\right\} \Big/ \eta \tag{11}$$

where the numerator is the total energy in the signal and the denominator is the rms noise power per hertz. With the parameters from Table I, a S/N of 2575 is obtained, indicating that the system is capable of resolving a 5-mm object with considerable assurance.

VI. Summary

Microwave-induced thermoelastic pressure waves appear to possess some unique features that may allow them to be

used in systems that permit noninvasive imaging of tissue characteristics which are not identifiable by other techniques. The system design has gray level resolution of 256 levels and spatial resolution of 5×5 mm. Both of these resolutions are sufficient to provide necessary information for indicating the potential of microwave-induced thermoelastic imaging as a useful method for imaging biological tissues. The hybrid parallel/serial design yields good picture quality of reasonable cost, provided the object is quasi-stationary.

REFERENCES

[1] A. C. Kak, "Special issue on computerized medical imaging," *IEEE Trans. Biomed. Eng.*, vol. 28, pp. 49–234, 1981.

[2] G. L. Brownell, T. F. Budinger, P. C. Lanterbur, and P. L. McGreer, "Position tomography and nuclear magnetic resonance," *Science*, vol. 215, pp. 619–626, 1982.

[3] J. C. Lin, *Microwave Auditory Effects and Applications*. Springfield: Charles C. Thomas, 1978.

[4] R. G. Olsen, "Generation of acoustic images from the absorption of pulsed microwave energy," in *Acoustic Imaging*, vol. 11, J. P. Powers, Ed. New York: Plenum, 1982, pp. 53–59.

[5] R. G. Olsen and J. C. Lin, "Acoustic imaging of a model of a human hand using pulsed microwave irradiation," *Bioelectromagn.*, vol. 4, pp. 397–400, 1983.

[6] L. S. Gournay, "Conversion of electromagnetic to acoustic energy by surface heating," *J. Acoust. Soc. Am.*, vol. 40, no. 6, pp. 1322–1330, 1966.

[7] R. S. Cobbold, *Transducers for Biomedical Measurements: Principles and Applications*. New York: Wiley-Interscience 1974, pp. 170–174.

[8] Analog Devices, *Data Acquisition Data Book*. vol. 1, 1982, pp. 14–20.

[9] C. A. Vergers, *Handbook of Electrical Noise*. Blue Ridge, Summit: TAB, 1979.

[10] H. Taub and D. Schilling, *Principles of Communication Systems*. New York: McGraw-Hill, 1971.

James C. Lin was born in 1942 and received the B.S., M.S., and Ph.D. degrees in electrical engineering from the University of Washington in Seattle.

Presently, he is Head of the Department of Bioengineering at the University of Illinois at Chicago, where he also serves as a Professor of Bioengineering and of Electrical Engineering, and as Director of the College of Engineering Robotics and Automation Laboratory. He formerly held professorial appointments at Wayne State University in Detroit and the University of Washington. His publications have appeared in many journals and books, and include the book on *Microwave Auditory Effects and Applications* (Springfield: Thomas, 1978). He received an IEEE Transactions Prize Paper Award in 1976 and a National Research Service Award in 1982.

Professor Lin has been a scientific consultant to numerous private, state, and federal agencies. He is a member of the editorial board of *Bioelectromagnetics*, IEEE TRANSACTIONS ON MICROWAVE THEORY AND TECHNIQUES, *Journal of Microwave Power*, and *Journal of Environmental Pathology and Toxicology*. He has served on the IEEE Committee on Man and Radiation (COMAR), Robotics and Automation Council, IEEE/EMBS Committee on Biomedical Robotics (Chair), IEEE/MTT Committee on Biological Effects and Medical Applications (Chair), ANSI Subcommittee C95.4 (chaired its Dosimetry Working Group), and URSI/US National Committee of the National Academy of Science. He has been a member of the Board of Governors for the International Microwave Power Institute and the Board of Governors for the Bioelectromagnetics Society. He also served on the Governor's Task Force to Review Project Seafarer (Michigan) in 1976.

✤

Karen H. Chan photo and biography unavailable at time of publication.

Limitations of Imaging with First-Order Diffraction Tomography

MALCOLM SLANEY, STUDENT MEMBER, IEEE, AVINASH C. KAK, MEMBER, IEEE, AND LAWRENCE E. LARSEN, SENIOR MEMBER, IEEE

***Abstract*—In this paper, the results of computer simulations used to determine the domains of applicability of the first-order Born and Rytov approximations in diffraction tomography for cross-sectional (or three-dimensional) imaging of biosystems are shown. These computer simulations were conducted on single cylinders, since in this case analytical expressions are available for the exact scattered fields. The simulations establish the first-order Born approximation to be valid for objects where the product of the relative refractive index and the diameter of the cylinder is less than 0.35λ. The first-order Rytov approximation is valid with essentially no constraint on the size of the cylinder; however, the relative refractive index must be less than a few percent.**

We have also reviewed the assumptions made in the first-order Born and Rytov approximations for diffraction tomography. Further, we have reviewed the derivation of the Fourier Diffraction Projection Theorem, which forms the basis of the first-order reconstruction algorithms. We then show how this derivation points to new FFT-based implementations for the higher order diffraction tomography algorithms that are currently being developed.

Manuscript received October 12, 1983; revised March 9, 1984.

M. Slaney and A. C. Kak are with the School of Electrical Engineering, Purdue University, West Lafayette, IN 47907.

L. E. Larsen is with Microwaves Department, Walter Reed Army Institute of Research, Washington, DC 20012.

I. INTRODUCTION

DURING THE past ten years, the medical community has increasingly called on X-Ray computerized tomography (CT) to help make its diagnostic images. With

0018-9480/84/0800-0860$01.00 ©1984 IEEE